Variation in stream network relationships and geospatial predictions of watershed conductivity

Michael G. McManus[1,5], Ellen D'Amico[2,6], Elizabeth M. Smith[3,7], Robyn Polinsky[3,8], Jerry Ackerman[4,9], and Kip Tyler[3,10]

[1]Center for Environmental Measurement and Modeling, Office of Research and Development, United States Environmental Protection Agency, 26 West Martin Luther King Drive, Cincinnati, Ohio 45268 USA

[2]Pegasus Technical Services c/o United States Environmental Protection Agency, 26 West Martin Luther King Drive, Cincinnati, Ohio 45268 USA

[3]Water Division, United States Environmental Protection Agency, Region IV, 61 Forsyth Street Southwest, Atlanta, Georgia 30303 USA

[4]Laboratory Services and Applied Science Division, United States Environmental Protection Agency, Region IV, 980 College Station Road, Athens, Georgia 30605 USA

Abstract: Secondary salinization, the increase of anthropogenically-derived salts in freshwaters, threatens freshwater biota and ecosystems, drinking water supplies, and infrastructure. The various anthropogenic sources of salts and their locations in a watershed may result in secondary salinization of river and stream networks through multiple inputs. We developed a watershed predictive assessment to investigate the degree to which topology, landcover, and land-use covariates affect stream specific conductivity (SC), a measure of salinity. We used spatial stream network models to predict SC throughout an Appalachian stream network in a watershed affected by surface coal mining. During high-discharge conditions, 8 to 44% of stream km in the watershed exceeded the SC benchmark of 300 μS/cm, which is meant to be protective of aquatic life in the Central Appalachian ecoregion. During low-discharge conditions, 96 to 100% of stream km exceeded the benchmark. The 2 different discharge conditions altered the spatial dependency of SC among the stream monitoring sites. During most low discharges, SC was a function of upstream-to-downstream network distances, or flow-connected distances, among the sites. Flow-connected distances are indicative of upstream dependencies affecting stream SC. During high discharge, SC was related to both flow-connected distances and flow-unconnected distances (i.e., distances between sites on different branches of the network). Flow-unconnected distances are indicative of processes on adjacent branches and their catchments affecting stream SC. With sites distributed from headwaters to the watershed outlet, the extent of impacts from secondary salinization could be better spatially predicted and assessed with spatial stream network models than with models assuming spatial independence. Importantly, the assessment also recognized the multiscale spatial relationships that can occur between the landscape and stream network.

Key words: streams, monitoring, spatial autocorrelation, specific conductivity, surface mining, block kriging, discharge, secondary salinization

Secondary salinization, the increase of anthropogenically-derived salts in freshwaters, threatens freshwater biota and ecosystems, drinking water supplies, and infrastructure (Cañedo-Argüelles et al. 2013, Kaushal et al. 2018). The variety of anthropogenic sources of salts and their locations in a watershed may result in secondary salinization of river and stream networks through multiple inputs. These salt inputs into freshwaters include de-icers for roadways, sidewalks, and parking lots; weathering of concrete infrastructure; wastewater treatment plants; agricultural irrigation; oil and gas extraction; and surface coal mining, particularly mountaintop mining and valley fills (MTM/VF) (Cañedo-Argüelles et al. 2013, Griffith 2014, Moore et al. 2017). Salt inputs increase the salinity of freshwater, measured

E-mail addresses: [5]mcmanus.michael@epa.gov; [6]damico.ellen@epa.gov; [7]smith.elizabeth@epa.gov; [8]polinsky.robyn@epa.gov; [9]ackerman.jerry@epa.gov; [10]tyler.kip@epa.gov

DOI: 10.1086/710340. Received 25 September 2018; Accepted 17 March 2020; Published online 10 September 2020; Associate editor, Matthew Baker.

as specific conductivity (SC), and negatively affect the physiology and ecology of freshwater biota (Cañedo-Argüelles et al. 2013, Griffith 2017, Timpano et al. 2018a).

The ecological impacts of secondary salinization on stream biota have been a focus of research in the Central Appalachian (CAP) ecoregion of the eastern United States. In this region, 7% of the total land area (5900 km^2) was mined over the 4-decade period from 1976 to 2015. This intense and persistent land use has dramatically affected the landscape and streams (Pericak et al. 2018). MTM/VF, a type of surface mining, results in increased stream SC in the CAP ecoregion (Merriam et al. 2011, Bernhardt et al. 2012, Griffith et al. 2012, Timpano et al. 2018b). SC in reference streams tends to be low and consistent, whereas SC in streams affected by MTM/VF tends to be ~10-fold higher and more variable (Green et al. 2000, Hartman et al. 2005, Merricks et al. 2007, Pond et al. 2008, Lindberg et al. 2011, Merriam et al. 2011, Bernhardt et al. 2012, Timpano et al. 2015, Boehme et al. 2016, Merriam and Petty 2016, Nippgen et al. 2017). Increased stream SC is associated with increased concentrations of sulfate, calcium, magnesium, and bicarbonate ions (Griffith et al. 2012, Timpano et al. 2015, 2018b, Boehme et al. 2016) and the loss of sensitive macroinvertebrates, particularly Ephemeroptera species (Pond et al. 2008, 2014, Lindberg et al. 2011, USEPA 2011, Bernhardt et al. 2012, Timpano et al. 2015, 2018a, Boehme et al. 2016, Clements and Kotalik 2016). The altered chemistry of mined streams is also associated with depressed productivity of sensitive taxa when SC increases during summer baseflows (Voss and Bernhardt 2017). Most ecological studies conducted previously have used catchments of small spatial extents from 0.50 to 50 km^2 in size. However, a stream survey of 30 watersheds at the sub-basin level (Hydrologic Unit Code [HUC] 8), ranging in size from ~750 to 6000 km^2, also observed a multimetric benthic invertebrate index negatively related to SC (McManus et al. 2016). Nonetheless, none of these studies incorporated the spatial configuration of the watershed's stream network from headwaters to outlet.

Griffith et al. (2012) and Johnson et al. (2010) noted the need for longitudinal studies of SC over a larger spatial extent to better understand cumulative effects of MTM/VF on downstream waters. A watershed's stream network is dynamic with influences such as meteorological events, seasonal variability, and multi-annual oscillations causing expansion and contraction of the network along longitudinal, lateral, and vertical dimensions (Stanley et al. 1997, Godsey and Kirchner 2014, Costigan et al. 2016, Fritz et al. 2018). Against this backdrop of stream dynamics, spatial influences on water chemistry measurements at sites throughout the network can be caused by processes occurring within the network, across the catchments surrounding the network, or a combination of both (McGuire et al. 2014, Rushworth et al. 2015). The hierarchical, dendritic, and directional qualities of stream networks are now better incorporated with newer geostatistical methods of spatial stream network (SSN) modeling (Peterson and Ver Hoef 2010, Peterson et al. 2013, Isaak et al. 2014, Ver Hoef et al. 2014). SSN models often outperform traditional, non-spatial models that assume spatial independence across sites in a dendritic network. Because SSN models do not assume spatial independence, they are better than non-spatial models at fitting data from topologically-connected observations and using spatial relationships to make predictions (Frieden et al. 2014, Isaak et al. 2014, 2016, Scown et al. 2017). SSN modeling is versatile because it can estimate relationships between a response variable and predictor variables or covariates, predict the response variable at unsampled locations, and use a method known as block kriging (BK) to predict an average or total for different portions of the stream network (Ver Hoef et al. 2006, Isaak et al. 2014, 2016, Ver Hoef et al. 2014).

SSN analysis uses the spatial autocorrelation of measurements collected from sites distributed over the stream network by incorporating spatial autocovariance models to address the different distance relationships among sites, that is, Euclidean and network distances (Ver Hoef et al. 2006, Ver Hoef and Peterson 2010). Examining spatial autocorrelation of stream chemistry as a function of Euclidean, or straight-line, distances among sites incorporates traditional geostatistical autocovariance models (Ver Hoef and Peterson 2010). For example, sodium concentrations in Hubbard Brook Valley, New Hampshire, USA, and strontium concentrations in Nushagak River, Alaska, USA, exhibited broad-scale gradients related to Euclidean distances, with those patterns attributed to geological features in the watersheds (McGuire et al. 2014, Brennan et al. 2016). Network distances, in contrast, are more suitable for water quality variables, which have spatial autocorrelation structured by the network. There are 2 types of stream network distance: flow-connected distance, which refers to sites on the network that have an upstream-to-downstream relationship, and flow-unconnected distance, which refers to sites that are on different branches of the network with confluence downstream (Peterson and Ver Hoef 2010, Ver Hoef and Peterson 2010). Autocorrelation can be restricted to flow-connected distances by specifying a tail-up autocovariance model, which might be appropriate for stream chemistry variables having passive downstream diffusion, serial dilution, or active advection of solutes, such as total phosphorus concentration (Peterson and Ver Hoef 2010, Ver Hoef and Peterson 2010, Isaak et al. 2014, Scown et al. 2017). Flow-connected and flow-unconnected distances can be modeled together with a tail-down autocovariance model. One example where this method could be useful is for fish abundance among sites, given that fish can move upstream and downstream throughout the network (Ver Hoef and Peterson 2010, Isaak et al. 2014, 2016). The ability to specify and combine different distance relationships and autocovariances illustrates the versatility of SSN modeling for

predictive assessments of water quality in a watershed's stream network.

Understanding how spatial variation in a stream network is manifested under different hydrologic conditions can help identify whether processes occurring instream, on the landscape, or some combination of the 2 are influencing predictive assessments of watersheds. In this study, we developed a watershed predictive assessment to examine the degree to which topology, land-cover, and land-use covariates affect stream SC from the headwaters to the outlet of a CAP watershed's stream network where surface mining occurs. Spatial autocorrelation in SC has previously been examined in stream networks by geostatistical summaries and graphics (Dent and Grimm 1999, McGuire et al. 2014) and through SSN modeling (Peterson et al. 2006, Ver Hoef and Peterson 2010). However, there have not been any studies to date that have characterized SC in a single stream network under varying hydrologic conditions with the purpose of comparing spatial and non-spatial models to predict the effects of stream SC on stream biota. We leveraged monitoring data to ask the following: 1) what covariates, or predictor variables, if any, are consistently selected among models to predict SC in the stream network?; 2) how does hydrologic variability alter the nature and degree of spatial autocorrelation in SC?; 3) to what degree does an SSN model improve the accuracy and precision of SC prediction over a non-spatial multiple linear regression (MLR) model?; and 4) what portions of the stream network likely have SC levels that would affect macroinvertebrate communities?

METHODS

To answer our research questions, we designed a monitoring study to collect water quality data quarterly over 2 y from the same stream network of sites under high- and low-discharge periods. We modeled observed SC as function of landform, land-cover, and land-use covariates using non-spatial MLR and SSN methods for each of the 8 monitoring periods. By fitting different spatial autocovariance models, we evaluated if hydrologic variability affected spatial autocorrelation in SC. We compared MLR and SSN models regarding model fit and predictive performance. Finally, we used BK to predict what portions of the stream network likely have SC levels that would affect macroinvertebrate communities.

Study area and monitoring design

The Right Fork of Beaver Creek (RFBC) is a 400-km^2 watershed in the Eastern Coalfield Region of the Central Appalachians, Kentucky, USA, in ecoregion 69d, the Dissected Appalachian Plateau (Omernik 1987). It flows north through Knott and Floyd Counties and includes 3 HUC12 subwatersheds: Upper, Middle, and Lower (050702030101, 050702030102, and 050702030103, respectively). The watershed is home to 10,079 people and has a population density of 25 people/km^2 (USEPA 2019). Populated places in the watershed are often clustered in the stream valleys, particularly along the lower RFBC mainstem. In addition to commercial and residential development, other land uses in the watershed include surface coal mining and valley filling, underground coal mining, oil and gas production, and forestry.

We established 60 monitoring sites throughout the ~545 stream km study area based on National Hydrography Dataset high-resolution data of RFBC (USGS 2016; Fig. 1). We chose site locations to create a longitudinal profile of the watershed that was well-suited for SSN analysis (Som et al. 2014). Site locations included headwaters (i.e., 1st- and 2nd-order streams, 29%), 3rd-order (33%), 4th-order (25%), and 5th-order (13%) streams, including the outlet (site RFBC1). Twenty-five % of the site locations were on the mainstem of the RFBC watershed, and 17% of the sites were clustered near confluences. We sampled the monitoring sites quarterly from December 2012 to August 2014 over 3 to 4 consecutive days ($n = 8$ sample periods).

We measured the in-situ physicochemistry variables (e.g., SC, temperature, dissolved oxygen, pH, and turbidity) with a 6920-V2 multi-parameter sonde (Yellow Springs Instruments, Yellow Springs, Ohio). We collected stream discharge measurements with a Flowtracker® handheld Acoustic Doppler Velocimeter® (SonTek, San Diego, California) at each site during the first 4 sampling periods. However, this handheld instrument could not be safely used by field personnel wading at discharges greater than 6555 L/s, which resulted in right-censored discharge observations at 1 site, 3 sites, and 5 sites on the RFBC mainstem during December 2012, March 2013, and August 2013 sampling periods, respectively. For the last 4 sampling periods, we avoided censored observations at non-wadeable sites by measuring discharge with an OceanScience Q-Boat 1800P™ with a Rio Grande Acoustic Doppler Current Profiler (Teledyne Marine Incorporated, Thousand Oaks, California). We also recorded global positioning system coordinates for each site.

Geoprocessing of the stream network and covariates

We geoprocessed the spatial information of both the stream network and covariates for SSN analysis. The same geoprocessing was done for the monitoring sites and for the prediction sites used in BK (see below). To produce the landscape network (LSN) with a single streamline for each reach, we reconditioned, or simplified, the digital stream network of the RFBC with the STARS 2.0.4 toolbox (Peterson and Ver Hoef 2014) in ArcGIS (version 10.3, Environmental Systems Research Institute, Redlands, California). The LSN is a geodatabase containing a number of relationship tables that report the topological relationships, such as flow direction among all the reaches in the stream network and branching structure of the network (Peterson

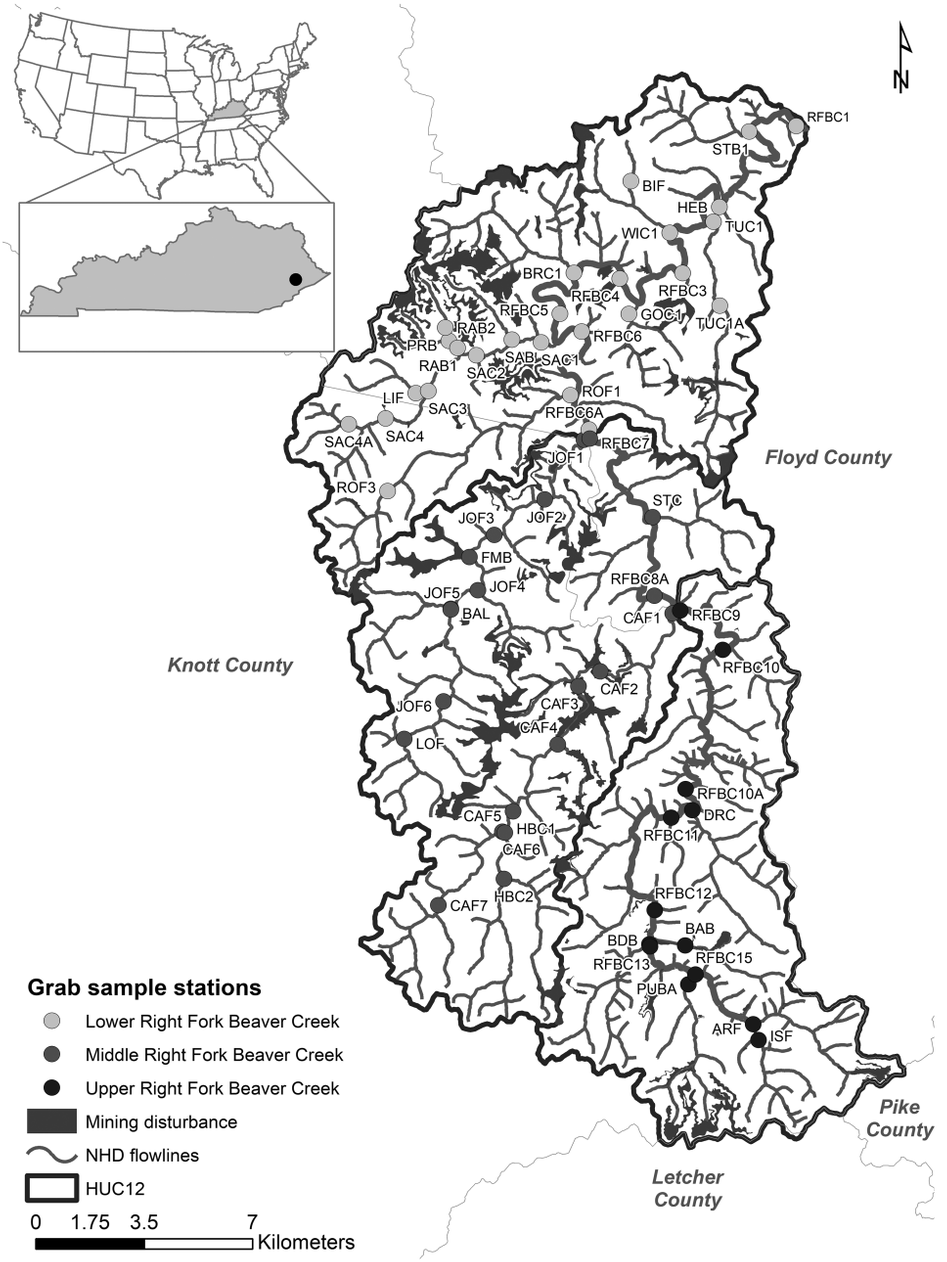

Figure 1. The 60 sample locations within the Right Fork of Beaver Creek (RFBC) watershed, eastern Kentucky, USA, which includes 3 hydrologic unit code (HUC12) watersheds—050702030101, 050702030102, and 050702030103—for the Upper, Middle, and Lower watersheds, respectively. The stream flows north, and its outlet is at RFBC1. NHD = National Hydrography Dataset.

and Ver Hoef 2014). A 1-to-1 relationship exists between each reach and its surrounding landscape, the reach contributing area (RCA).

We derived covariates from geospatial data characterizing landform, land cover, and land use (Table 1) and associated them with their corresponding RCA sites. We included elevation and slope (% rise) because the weathering of natural geological inputs to stream SC might vary with landform (USGS 2013). We also included proportion of forested land cover (MRLC 2011) and land-use covariates: housing density (USCB 2010), road km (USCB 2016), and proportion surface mining disturbance (hereafter proportion mined) based on National Agricultural Imagery Program (NAIP) data (USDA 2010). Land-cover and land-use covariates were expressed cumulatively. That is, we summed the total amount or area of each covariate over the RCA and divided by the accumulated area as we progressed downstream.

Table 1. Description and sources of land-form, land-use, and permit covariates. Geoprocessing describes the steps to create the covariate for each reach contributing area (RCA). NED = National Elevation Dataset, DEM = digital elevation model, NPDES = National Pollutant Discharge Elimination System permits.

Covariate	Source	Geoprocessing
Average elevation	USGS 2013 NED 10-m DEM (Nationalmap.gov/elevation.html)	Average elevation within an RCA. Calculated using zonal statistics.
% rise	USGS 2013 NED 10-m DEM (Nationalmap.gov/elevation.html)	Average % rise of the elevation/RCA. Calculated using zonal statistics.
Housing density	USCB 2010 (https://www.census.gov/geographies/mapping-files/time-series/geo/carto-boundary-file.html)	Averaged 2010 Census housing unit counts by Census block area. Used zonal statistics with the average housing unit to calculate housing density/RCA.
Road kilometer	USCB 2016 (www.census.gov/geographies/mapping-files/time-series/geo/tiger-line-file.html)	Total length (km) of roads within an RCA divided by the area of an RCA.
Proportion forested	MRLC 2011 (www.mrlc.gov/data)	Proportion of RCA that has forested land cover. Used the tabulate area tool in ArcMap to calculate the area of forested land (a combination of deciduous, evergreen, and mixed forest types).
Non-coal NPDES	J. Blanset, Watershed Management Branch, Kentucky Division of Water, personal communication, 2016	Count of non-coal NPDES permits/RCA, converted to presence/absence. Non-coal NPDES permits were selected using the Standard Industrial Classification (SIC) attribute (SIC < or > 1221). SIC = 1221, represents bituminous and lignite surface mining.
Proportion mined	USDA 2010 (earthexplorer.usgs.gov)	The proportion of the RCA that was mined. Mining layer was created through hand digitization of land exhibiting disturbance from surface mining: clearly deforested, scarred and included distinct terracing, fills, and mining roads. These areas frequently corresponded to GIS layers of surface mining permit boundaries or points, with most of those permits being from 1980 through early 2011.
Coal outfall density	K. Gale, Division of Mine Reclamation and Enforcement, Kentucky Department of Natural Resources, personal communication, 2016	Count of NPDES surface coal outfalls/RCA

We created 2 additional covariates based on National Pollutant Discharge Elimination System (NPDES) permits: presence or absence of non-coal permits/RCA and counts of coal permits/RCA (Table 1). We developed the 1st covariate from a point data layer of NPDES permits (J. Blanset, Watershed Management Branch, Kentucky Division of Water, personal communication), which we spatially joined to the RCAs. We selected non-coal permits, such as wastewater treatment plants, and excluded permits associated with bituminous and lignite surface mining. We converted counts to presence/absence because nearly ¼ of these counts were 0. We developed the 2nd covariate from Discharge Monitoring Reports of surface mine outfalls monitored by coal companies (K. Gale, Division of Mine Reclamation and Enforcement, Kentucky Department of Natural Resources, personal communication), which we also spatially joined to the RCAs. Both coal and non-coal permit covariates were expressed as cumulative variables. The response variable for the SSN analysis was SC for each site ($n = 60$) from a specific sampling period, which we log transformed to account for skewness in the data.

Spatial stream network analysis

We completed our statistical analysis in 2 steps to identify covariates and compare spatial autocovariances that describe spatial relationships among monitoring sites in the network. The 1st step addressed which covariates, if any, were consistently selected to predict SC, and the 2nd step addressed if the nature and degree of spatial autocorrelation in SC is affected by hydrologic variability, our 1st and 2nd research questions, respectively. For each sampling period, we followed Ramsey and Schafer (2002) in our modeling strategy to adjust for a large set of covariates. We approached model fitting and selection to account for as much variation in SC by non-coal covariates first and then consider the mining covariates. We also aimed to avoid overfitting the model. We note that other modeling approaches might identify a different set of covariates as the best model. We 1st developed a non-spatial MLR of SC with only the non-coal covariates: elevation, % rise, housing density, proportion forested, road km, and presence/absence of non-coal permits. This analysis used best-subsets regression (Furnival and Wilson 1974) from

the package *bestglm* (McLeod and Changjiang 2018) in R (version 3.6.2; R Project for Statistical Computing, Vienna, Austria). We used Akaike information criterion (AIC) to select the best set of covariates for each sampling period. For the initial model of non-coal covariates, we selected the model with the minimum AIC value. We then used Akaike weights to compare 3 models: non-coal covariates, non-coal covariates plus coal outfall density, and non-coal covariates plus proportion mined. Akaike weight values range from 0 to 1 with the sum of the weights of all of the candidate models equaling 1 (Symonds and Moussalli 2011). We used the *BMhyd* package (version 1.2-8; Jhwueng and O'Meara 2015) in R to calculate the weights. In all cases, models that included the proportion mined had a much greater Akaike weight (0.76–1.0) compared to the other 2 models (Appendix S1). Diagnostic plots of the proportion-mined models showed some curvilinear patterns in the residuals, suggesting a quadratic of mine disturbance could improve model fit. Quadratic models had greater Akaike weights (0.98–1.0) and better diagnostic plots than those with solely linear terms (Appendix S1). We also examined the variance inflation factor to see if any covariates exceeded the threshold of 10, which indicates multicollinearity (Dormann et al. 2013). We then used the final 8 MLR models, 1 for each sampling period, for SSN model fitting and predictions (Appendix S2).

SSN models incorporate topological configuration and Euclidean, flow-connected, and flow-unconnected distances by specifying spatial autocovariance functions (Peterson and Ver Hoef 2010, Ver Hoef and Peterson 2010). From the spatial autocovariance functions, 3 parameters—nugget, sill, and range—can be estimated by plotting a semivariogram that shows how semivariance, and hence autocorrelation strength, changes as a function of distance between sites (Peterson et al. 2006). The nugget, or independent error term, describes spatial variation occurring at a distance smaller than the shortest distance among pairs of sites. The sill is the value at which the autocovariance plateaus as a function of distance. The range is the distance beyond which little or no spatial autocorrelation occurs (Peterson et al. 2006, Krivoruchko 2011). We used the *SSN* package (Ver Hoef et al. 2014) in R with restricted estimate maximum likelihood to fit a total of 15 autocovariance models for each sampling period. We fitted all 1-way, 2-way, and 3-way combinations of Euclidean, tail-up, and tail-down autocovariance models and crossed each combination with either an exponential or spherical structure, plus the MLR that assumed independent observations. All 3 types of autocovariance may need to be included in model building because of the complex and multi-scale patterns that occur in stream datasets (Peterson and Ver Hoef 2010, Frieden et al. 2014). The exponential and spherical structures represent the shape of the semivariogram from which the geostatistical parameters of nugget, sill, and range were estimated. We compared Akaike weights of models having the different covariance structures. For each of the 8 sampling periods, we selected a final SSN model that had the highest weight and lowest root mean square prediction error (RMSPE). The RMSPE is produced from a leave-1-out cross validation used to evaluate model performance (Ver Hoef et al. 2014). We compared the RMSPE of the SSN models to the RMSPE of their corresponding non-spatial MLR models to examine the difference between their predictive performance, thereby addressing our 3rd research question.

Predicting stream segments with high SC

To address our 4th research question, we used BK to compare SC predictions from different segments of the stream network and identify portions that likely have SC levels high enough to affect macroinvertebrate communities. BK can be used to identify stream segments that either differ or are similar to nearby streams. We used a Python script to place prediction points at every ~100 m throughout the RFBC network because BK requires a set of spatially-dense points. We then used universal kriging to predict SC at

Table 2. Summary statistics of land-form, land-use, and permit covariates for the 60 sites in the Right Fork of Beaver Creek Network. Min = minimum, Max = maximum, Qu = quartile, NC NPDES = non-coal National Pollutant Discharge Elimination System permits.

Covariate	Min	1st Qu	Median	Mean	3rd Qu	Max
% rise	0.0	2.1	5.7	7.2	10.1	24.2
Average elevation (m)	195.0	208.0	230.0	237.0	264.0	312.0
Housing density (#/km^2)	3.4	7.6	8.8	9.5	10.5	22.8
Road kilometer (km/km^2)	0.36	1.06	1.21	1.21	1.36	2.10
Proportion forested	0.579	0.793	0.826	0.812	0.853	0.918
NC NPDES density (#/km^2)	0.00	0.00	0.028	0.080	0.117	0.451
Proportion mined	0.00	0.028	0.059	0.072	0.083	0.303
Coal outfall density (#/km^2)	0.00	0.25	0.66	1.24	1.04	9.19

5120 points. Universal kriging incorporates predictions from the covariates, with adjustments for spatial autocorrelation, along with the SSN models that had the highest Akaike weights and lowest RMSPE (Cressie 1993). To check for unreasonable predictions and extrapolations, we compared the minimum and maximum values of the covariates at the prediction sites to the minimum and maximum values of the covariates at the 60 monitoring sites (Table 2). By predicting at such a high density of points on the network, it was then possible to integrate predicted SC over different portions of the network through BK. This technique allowed us to predict average SC and estimate a 95% prediction interval for specific portions of the network within each sampling period. We used BK over the 60 monitoring site locations and integrated the SC predictions from universal kriging that were upstream of the monitoring site locations to predict an average SC for those portions of the network. We compared those predicted average SC and 95% confidence intervals to the conductivity benchmark of 300 µS/cm for CAP streams (USEPA 2011) to identify which parts of the network were consistently below or above that benchmark over the 8 sample periods. This comparison identified what portions of the stream network likely had SC levels that would affect macroinvertebrate communities.

RESULTS

Exploratory data analysis

We visually classified the quarterly synoptic samples into 2 groups, high stream discharge and low SC vs low stream discharge and high SC (Fig. 2A, B), based on stream discharge and SC descriptive statistics. When discharge was high (December 2012, March 2013, August 2013, and April 2014; median = 240 L/s), SC had a median value of ≤450 µS/cm. When discharge was low (June 2013, November 2013, June 2014, and August 2014; median = 40 L/s), SC had a median value of ≥800 µS/cm. SC minimum (66 µS/cm) was recorded in August 2013 (a high-discharge sample) at the LIF site, a tributary of Saltlick Creek in the Lower RFBC (see Fig. 1 for site locations), and SC maximum (2445 µS/cm) was recorded in November 2013 (a low-discharge sample) at the FMB site, a tributary of Jones Branch in the Middle RFBC. The LIF site also recorded the discharge minimum (0.02 L/s) in August 2014,

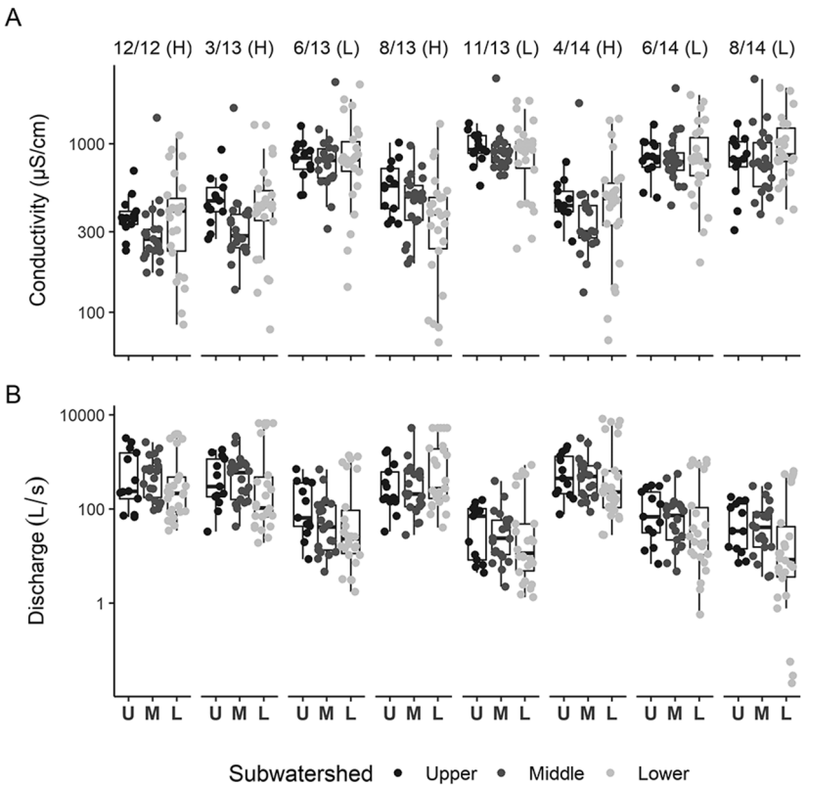

Figure 2. Box plots of specific conductivity (µS/cm) (A) and stream discharge (L/s) (B) for the Upper (U), Middle (M), and Lower (L) Right Fork of Beaver Creek watersheds for each of the 8 sample periods (month/year). H indicates a high-discharge sample period, and L indicates a low-discharge sample period. The thick horizontal line is the median, the bottom of the box is the 1st quartile, the top is the 3rd quartile, and the vertical lines from each box extend to 1.5-fold greater than the interquartile range. The dots are the observed values.

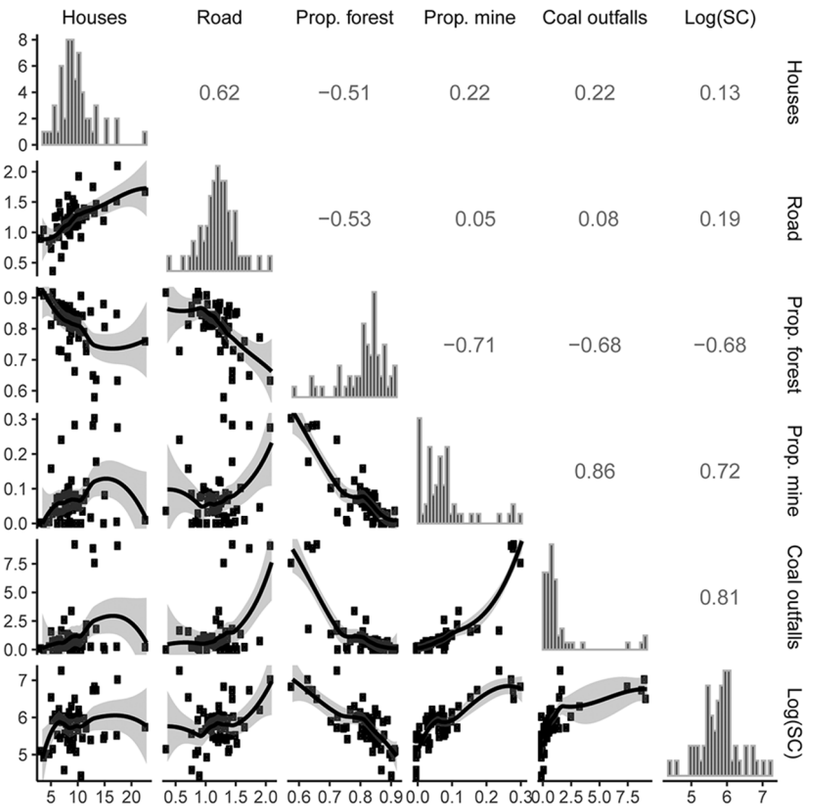

Figure 3. Scatter plot matrix of land-use, land-cover, and permit covariates—housing density (Houses, #/km^2), road kilometer (Road, km/km^2), proportion forested (Prop. forest), proportion mined (Prop. mine), and coal outfall density (Coal outfalls, #/km^2)—and log of specific conductivity (SC) from the December 2012 sample period for the 60 sites in the Right Fork of Beaver Creek network. Spearman rank correlations are shown in the upper matrix, and histograms appear along the diagonal. A locally weighted smoothing (LOESS) line, shown in black with a gray band, indicates the 95% confidence interval of the LOESS line.

which corresponded to that site's maximum SC (348 μS/cm). Discharge maximum (8210 L/s) was recorded at the watershed outlet (the RFBC1 site in the Lower RFBC) in April 2014.

Across the 8 sampling periods, the coal covariates had the most consistent association with SC (Fig. 3, Table 3, Appendix S1). The strongest positive correlations were between SC and the 2 mining covariates, proportion mined (ρ = 0.65–0.81) and coal outfall density (ρ = 0.61–0.85). The strongest negative correlation was between SC and proportion forested (ρ = −0.72 to −0.37). Housing density and road km were positively correlated with each other

Table 3. Spearman rank correlations between log specific conductivity (SC) from each of the 8 sample periods and land-use, land-cover, and permit covariates for the 60 sites in the Right Fork of Beaver Creek Network. H indicates a high-discharge sample period, and L indicates a low-discharge sample period.

Log(SC)	Housing density	Road kilometer	Proportion forested	Proportion mined	Coal outfall density
Dec 2012 (H)	0.13	0.19	−0.68	0.72	0.81
Mar 2013 (H)	0.08	0.19	−0.70	0.76	0.78
Jun 2013 (L)	0.14	0.06	−0.51	0.76	0.72
Aug 2013 (H)	0.14	−0.11	−0.37	0.65	0.61
Nov 2013 (L)	0.08	0.05	−0.54	0.80	0.75
Apr 2014 (H)	0.17	0.17	−0.72	0.81	0.85
Jun 2014 (L)	0.09	0.03	−0.52	0.78	0.74
Aug 2014 (L)	0.04	−0.01	−0.50	0.75	0.68

(ρ = 0.62). Both had weak associations with SC (ρ = −0.11–0.19), as did the land-form covariates of average elevation (ρ = −0.36–0.06) and % rise (ρ = −0.08–0.12) (Appendix S1).

MLR and SSN models

Non-spatial MLR modeling produced 3 results. First, models with the proportion-mined covariate, which had a positive slope, always had the greatest Akaike weights compared to either the non-coal covariates alone or non-coal covariates plus coal outfall density (Appendix S1). Adding coal outfall density produced no change in the weights of the non-coal covariate-only models. Models with the proportion-mined covariate had Akaike weights that ranged from 0.759 (August 2013) to 0.999 (June 2014). Second, adding the quadratic term for proportion mined produced models with Akaike weights ranging from 0.982 to 0.999 compared to non-coal covariates plus proportion-mined models with weights of 0.001 to 0.018 (Appendix S1). Third, proportion mined and its quadratic term were always selected in the MLR models across all 8 sampling periods (Table 4). Among the other covariates, proportion forested was selected most often and had a negative slope in 4 of the 8 sampling periods. Those negative slopes, which always occurred during high-discharge, low-SC periods, differed from 0 in December 2012, March 2013, and April 2014, but not in August 2013. All of the non-coal covariates selected in the non-spatial MLR models had variance inflation factors <10 (Appendix S1), indicating that they were not affected by multicollinearity. The positive relationship between proportion mined and SC remained when we modeled for spatial autocorrelation in the SSN analysis, but that was not always the case with the slopes of other covariates (Table 4).

Specifying spatial autocovariance models through the SSN analysis always fit the data better, based on greater Akaike weights, compared to non-spatial MLR models; however, different autocovariances were selected under different stream discharge conditions (Table 4, Appendix S3). For periods with high stream discharge (December 2012, March 2013, August 2013, and April 2014) both tail-up and tail-down autocovariance models were selected, and Akaike weights for the SSN models were 1.0 vs <0.001 for the MLR models. The tail-up and tail-down autocovariance models were also selected for November 2013 (low stream discharge), with an Akaike weight of 0.966 vs 0.034 for the MLR model. For the 3 summer periods with low stream discharge (June 2013, June 2014, and August 2014), the tail-up model was selected, and the Akaike weights were 0.670, 0.993, and 0.999, respectively.

We used leave-1-out cross validation to evaluate MLR and SSN model performance (Table 4). The SSN models from the high-discharge periods had 58 to 85% lower RMSPE than their corresponding MLR models. For the low-discharge periods of November 2013 and August 2014, the SSN models had ~18% lower RMSPE than MLR models. In both June 2013 and June 2014 (low discharge), the RMSPE was similar for SSN and MLR models. For the SSN models, semivariogram range, the distance beyond which little or no spatial autocorrelation in SC occurred, was 57 to 246 km.

The variance decomposition differed markedly between the SSN and MLR models (Table 5). In the SSN models, the covariates accounted for 53 to 79% of the variation in the data, and in the MLR models, covariates accounted for 62 to 74% of the variation. The nugget, or proportion of unexplained variation in the data, never exceeded 14% for the SSN models but was 26 to 38% for the MLR models. When tail-up and tail-down autocovariances were specified in 5 of the SSN models, they accounted for 21 to 31% of the variation. When only tail-up autocovariances were specified in the other 3 SSN models, they accounted for 33 to 42% of the variation. This difference in variance decomposition between the SSN and MLR models showed that spatial structure explained a sizeable portion of SC variation in the RFBC stream network.

Block kriging of SC

The % of stream km exceeding the 300 μS/cm benchmark, the subject of our 4th research question, is based on average SC and 95% prediction intervals from BK (Figs 4, S1A, B). During year 1, which had 3 high-discharge periods and 1 low-discharge period, 10 to 44% of stream km exceeded the benchmark during high discharge. During low discharge (June 2013), 98% of stream km exceeded the benchmark. During year 2, which had 3 low-discharge periods and 1 high-discharge period, 96 to 100% of stream km exceeded the benchmark during low discharge. During high discharge (April 2014), 8% of stream km exceeded the benchmark.

At times, extrapolations of the 5120 predictions from universal kriging occurred when the values of the covariates for those predicted points exceeded the covariate values of the 60 monitoring sites. The extrapolation of proportion mined produced unrealistically-low point predictions of SC, such as 0 μS/cm in June 2014, which was the result of a few predicted sites with high proportion-mined values coupled with the use of the quadratic function. For proportion mined, 5% of the predicted sites exceeded the maximum of the observed sites, but no extrapolation occurred at the lower limit because both predicted and observed sites had the same minimum value of 0. The other land-use covariates ranged in the percentages of prediction sites that exceeded the maximum or were less than the minimum values at observed sites: housing density: 2% predicted > observed, 5% predicted < observed; proportion forested: 18% predicted > observed, 4% predicted < observed; road km: 6% predicted > observed, 24% predicted < observed. The maximum road covariate from the 60 observed sites in the model was 2.1 km, but the maximum at a prediction site

Table 4. Parameter estimates for spatial stream network (SSN) and multiple linear regression (MLR) models fit to specific conductivity at 60 sites in the Right Fork of Beaver Creek network from the 8 sample periods. N/A = not applicable, NC NPDES Y/N = non-coal National Pollutant Discharge Elimination System permits yes/no, Quad. = quadratic, TU = tail-up, TD = tail-down, Weight = Akaike weight of the 2 models within a sample period, RMSPE = root mean square prediction error, * indicates $p < 0.05$. The – indicates a parameter was not selected for a particular model, and N/A indicates that the spatial autocovariance parameters are not applicable to the MLR models.

	Dec 2012		Mar 2013		Jun 2013		Aug 2013	
Model Parameters	SSN	MLR	SSN	MLR	SSN	MLR	SSN	MLR
Intercept	7.33*	7.17*	7.60*	8.45*	4.78*	4.94*	7.40*	5.06*
% rise	–	–	–	–	–	–	–	–
NC NPDES Y/N	–	–	0.05	−0.22*	–	–	–	–
Housing density	–	–	–	–	–	–	0.004	0.034
Road kilometer	–	–	–	–	0.38*	0.30*	–	–
Proportion forested	−2.72*	−3.22*	−2.69*	−3.46*	–	–	−2.54	−2.33
Average elevation	1.9×10^{-4}	3.4×10^{-3}*	–	–	0.003	0.003*	-4.3×10^{-5}	0.008*
Proportion mined	10.37*	9.23*	8.70*	9.48*	10.92*	10.71*	11.01*	15.75*
Quad. proportion mined	−22.21*	−20.58*	−16.17*	−23.02*	−21.94*	−21.39*	−23.78*	−45.15*
Autocovariance	TU, TD	N/A	TU, TD	N/A	TU	N/A	TU, TD	N/A
Spherical TU partial sill	0.064	N/A	0.097	N/A	0.089	N/A	0.061	N/A
Spherical TU range (km)	246.0	N/A	246.0	N/A	156.0	N/A	246.0	N/A
Spherical TD partial sill	0.226	N/A	0.124	N/A	–	N/A	0.724	N/A
Spherical TD range (km)	246.0	N/A	246.0	N/A	–	N/A	246.0	N/A
Weight	1.0	<0.001	1.0	<0.001	0.670	0.330	1.0	<0.001
RMSPE	0.162	0.296	0.169	0.312	0.318	0.327	0.276	0.437
	Nov 2013		Apr 2014		Jun 2014		Aug 2014	
	SSN	MLR	SSN	MLR	SSN	MLR	SSN	MLR
Intercept	5.42*	5.02*	8.88*	7.81*	5.58*	5.32*	6.18*	6.17*
% rise	–	–	–	–	–	–	0.006	0.011
NC NPDES Y/N	–	–	–	–	–	–	–	–
Housing density	–	–	–	–	–	–	–	–
Road kilometer	0.32*	0.33*	–	–	0.20	0.19	–	–
Proportion forested	–	–	−3.01*	−3.68*	–	–	–	–
Average elevation	0.002	0.004*	−0.005*	0.003	0.001	0.003*	–	–
Proportion mined	9.52*	11.54*	9.70*	11.96*	11.72*	10.94*	9.66*	9.02*
Quad. proportion mined	−20.22*	−28.02*	−20.10*	−30.14*	−29.05*	−23.91*	−18.01*	−16.44*
Autocovariance	TU, TD	N/A	TU, TD	N/A	TU	N/A	TU	N/A
Spherical TU partial sill	0.019	N/A	0.085	N/A	0.094	N/A	0.115[a]	N/A
Spherical TU range (km)	194.0	N/A	246.0	N/A	246.0	N/A	57.0[a]	N/A
Spherical TD partial sill	0.296	N/A	0.493	N/A	–	N/A	–	N/A
Spherical TD range (km)	246.0	N/A	246.0	N/A	–	N/A	–	N/A
Weight	0.966	0.034	1.0	<0.001	0.993	0.007	0.999	0.001
RMSPE	0.206	0.242	0.214	0.337	0.256	0.255	0.237	0.281

[a] Exponential TU autocovariance was selected.

was 8.2 km. This greater road covariate value resulted in an extrapolated prediction of 10,000 μS/cm in June 2013 at a few sites, which is unlikely, but greater observations of SC in the CAP have been reported (USEPA 2011).

Model extrapolation issues, such as unrealistic or extreme predictions, must be considered when interpreting model results. While we had extrapolations, these few extreme predictions had little effect when averaged over all the other sites in

Table 5. Variance components from multiple linear regression (MLR) and spatial stream network (SSN) models fit to specific conductivity at 60 sites in the Right Fork of Beaver Creek network from the 8 sample periods. The – indicates a parameter was not selected for a particular model.

		Proportion of variance in sampling period							
Model	Variance component	Dec 2012	Mar 2013	Jun 2013	Aug 2013	Nov 2013	Apr 2014	Jun 2014	Aug 2014
MLR	Covariates	0.74	0.74	0.63	0.62	0.71	0.74	0.71	0.63
MLR	Unexplained variance	0.26	0.26	0.37	0.38	0.29	0.26	0.29	0.37
SSN	Covariates	0.79	0.77	0.53	0.70	0.67	0.74	0.60	0.57
SSN	Tail-up spherical autocovariance	0.05	0.10	0.33	0.02	0.02	0.04	0.37	0.42[a]
SSN	Tail-down spherical autocovariance	0.16	0.13	–	0.28	0.29	0.22	–	–
SSN	Nugget	2.4×10^{-6}	3.0×10^{-5}	0.14	3.8×10^{-3}	0.02	5.7×10^{-5}	0.03	7.6×10^{-9}

[a] TU exponential was fit.

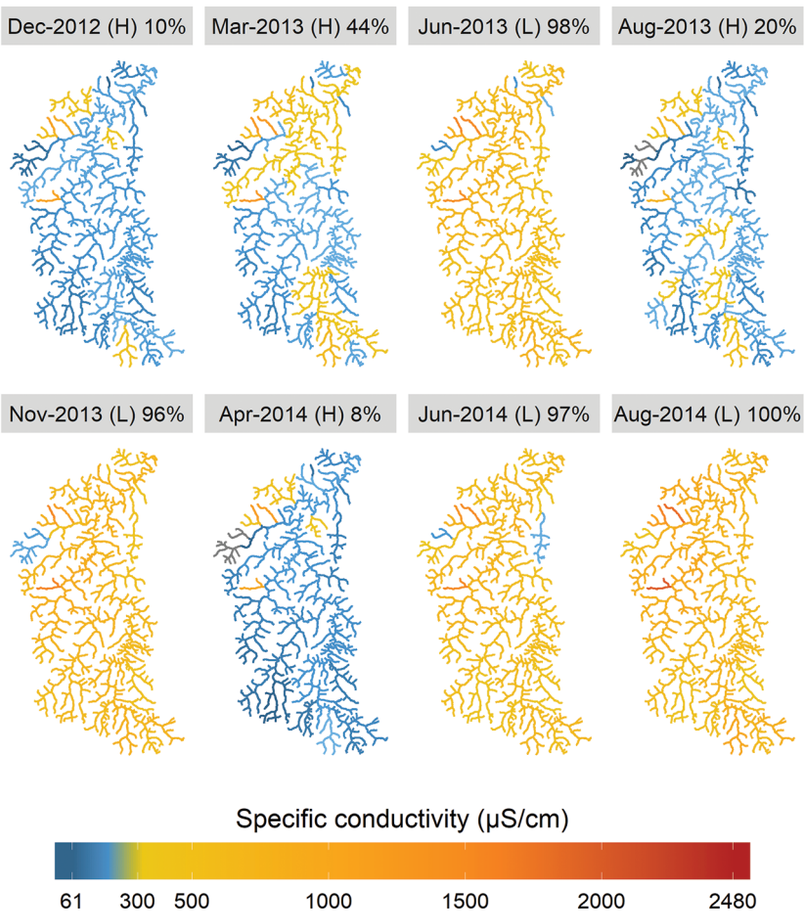

Figure 4. Block-kriged predictions of the lower 95% prediction limit of specific conductivity from spatial stream network models fit to each sample period. Percentages indicate what portion of the stream network had a lower 95% prediction limit greater than the specific conductivity benchmark of 300 µS/cm. H indicates a high-discharge sample period, and L indicates a low-discharge sample period.

the network to produce the BK predictions of SC. Extrapolations are not advantageous for any predictive model, but they can be minimized in an SSN study by examining the covariate distribution of the proposed observed and predicted sites (Scown et al. 2017, Marsha et al. 2018).

DISCUSSION

We modeled SC in an Appalachian stream network affected by surface coal mining and identified stretches with SC levels that exceeded a threshold for negative macroinvertebrate effects. These predictions revealed seasonal and discharge-related patterns in SC, but some portions of the stream network consistently exceeded the threshold. We assessed the effect of hydrologic variability on spatial autocorrelation in the model and found that, although flow-connected autocorrelation always influenced stream SC, flow-unconnected autocorrelation also influenced stream SC during high-discharge periods. To understand the degree to which mining and non-mining covariates influenced SC, we identified covariates that consistently affected SC in both non-spatial MLR and spatial SSN models. Finally, we compared MLR and SSN models in terms of their ability to predict SC. SSN models had better predictive performance, especially when stream discharge was high, which supports incorporation of spatial data into modeling for comprehensive analysis of mining impacts throughout stream systems.

Network predictions of SC

By modeling SC from headwaters to outlet of a stream network, we were able to accurately describe spatial variation in SC and make whole-network BK predictions of SC. To our knowledge, this is the first application of comparing BK predictions on a stream network to a water quality benchmark (Isaak et al. 2014). Our results add to prior predictive work on the effect of surface mining area on stream SC (Bernhardt et al. 2012, Merriam et al. 2015b) by incorporating the influence of spatial autocorrelation. Studies on the effects of surface mining on stream water quality and biota have often compared mined streams to reference streams and have focused on the extremes of SC distribution instead of looking at the gradient along the network (Pond et al. 2008, Timpano et al. 2015, Boehme et al. 2016, Voss and Bernhardt 2017). Geographically, these studies were done in the upper portion of the stream network in small catchments <50 km^2 in size. We found that some unmined tributaries in the RFBC exhibited low and less-variable SC, often below the benchmark. We also found that mined tributaries with high average SC and high variation were always above the benchmark, regardless of discharge condition. However, large portions of the RFBC stream network had average SC values intermediate to these extremes and exhibited seasonal patterns of SC related to discharge. Those network portions had high SC that surpassed the benchmark during low discharge, then either met the benchmark or were below it during high discharge.

Seasonal discharge effects on SC have implications for monitoring. For example, monitoring under high discharge could predict what portions of the network likely have chronically-high SC because those portions of the network would exceed the benchmark, such as the FMB stream reaches did, when the other portions of the network would likely be below the benchmark. Seasonal discharge effects on stream SC have been observed before in this region but were based on sampling small catchments (Johnson et al. 2010, Boehme et al. 2016, Nippgen et al. 2017, Voss and Bernhardt 2017, but see Timpano et al. 2018a), not over an entire network from headwaters to outlet as was done in this study.

Discharge-related shifts in SC over the network also have ecological implications. Elevated SC in small catchments is associated with ecological changes, including loss of sensitive Ephemeroptera species and decreased macroinvertebrate secondary productivity (Pond et al. 2008, Cormier et al. 2013, Boehme et al. 2016, Voss and Bernhardt 2017). In larger catchments up to ~200 km^2 in size, elevated SC has been hypothesized to affect quantity and quality of macroinvertebrate prey for some fishes (Hitt et al. 2016). Maps of average conductivity and confidence limits over a continuous stream network, rather than at discrete catchments, provide the means to investigate whether, and to what degree, such ecological patterns persist longitudinally. For example, one could use such maps to design a study to compare macroinvertebrate secondary productivity in portions of the network with variable SC to other portions of the network that have consistently-low or high SC. Such comparisons could identify the extent of the network over which secondary production differs from expectations based on the River Continuum Concept in which stream biotic structure and production and their relationships with the riparian zone are predicted to vary longitudinally along the stream network (Voss and Bernhardt 2017, Larsen et al. 2019).

Hydrologic variability and spatial autocorrelation

We found that hydrologic variability altered the degree and nature of spatial autocorrelation in SC. We observed the greatest semivariogram ranges at high discharge, and our finding of generally-smaller semivariogram ranges under summer low-discharge conditions is complementary to previous research (Dent and Grimm 1999). Additionally, our smallest and greatest semivariogram ranges encompass the range of spatial autocorrelation in SC in a stream network in southeast Queensland, Australia (Ver Hoef and Peterson 2010, Isaak et al. 2014). Our greatest semivariogram range was 4-fold greater than the largest upstream-to-downstream distance between monitoring sites, which indicates that at all

of the sites within the watershed are correlated with one another in terms of SC. Our smallest semivariogram range of ~60 stream km indicates that sites beyond that distance are uncorrelated in stream SC, but sites closer together were more correlated to one another. This smallest range occurred during the lowest summer discharge period.

Complex patterns in stream SC semivariance were related to flow-connected, flow-unconnected, and Euclidean distances, which suggests that a combination of fine-scale patchiness and broad-scale gradients affected stream SC (McGuire et al. 2014). We observed that SC among sites always had a flow-connected relationship, and that during high-discharge conditions a flow-unconnected relationship often also explained spatial variation. Our results are consistent with an SSN analysis of conductivity in streams of Queensland, Australia, in which Ver Hoef and Peterson (2010) fitted tail-up and tail-down spatial autocovariance models. They noted that the data had relatively-strong autocorrelation among flow-connected sites and weaker, but still substantial, autocorrelation among flow-unconnected sites. Most of our SSN analyses also fitted tail-up and tail-down spatial autocovariance models. However, during summer low-discharge conditions, only a tail-up model was selected, indicating that variation in SC was a function of upstream-to-downstream distances between sites and covariates. Correlations between SC at flow-connected sites is characteristic of hydrologic transport, such as active advection of conserved ions from weathering and land-use point sources, and of upstream spatial dependence (Isaak et al. 2014, McGuire et al. 2014). The amount of variation in SC explained by this longitudinal connectivity was substantial—from 33 to 42%. This spatial variation in SC under summer low-discharge conditions was likely due to mine disturbance containing valley fills that are a steady source of elevated SC and contribute a greater proportion to streamflow during baseflow periods (Nippgen et al. 2017). Spatial variation in stream SC may also be influenced by point sources, such as wastewater treatment plants, but our analysis did not partition that variation by point vs non-point sources.

Spatial variation in SC was also a function of distances between sites on other branches (flow-unconnected). Under all 4 high-discharge conditions, the tail-up and tail-down autocovariance models were selected over the other models, indicating that SC at high discharge was affected by both longitudinal transport and catchment processes (Peterson and Ver Hoef 2010, McGuire et al. 2014, Rushworth et al. 2015). For these high-discharge periods, flow-unconnected distances accounted for more variation than longitudinal connectivity, which may be because of catchment processes such as shallow subsurface flow, bank storage release, or overland flow (Fritz et al. 2018). The tail-up and tail-down models were also selected in the November 2013 sampling period, which had the lowest median discharge. Under that low discharge condition, the amount of variation explained by longitudinal connectivity was only 2% but was 29% for catchment processes. We infer that the lack of evapotranspiration after leaf-off in the autumn may have supported spatial variation in SC as a function of flow-connected and flow-unconnected distances even at low stream discharge. This inference is supported by previous research that showed that autumnal vegetation dormancy was associated with changes in stream discharge (Doyle 1991) and that leaf litter in streams was associated with increased stream SC (Slack and Feltz 1968). Additionally, groundwater seepages could have contributed to elevated SC, and, as Nippgen et al. (2017) observed, mined areas can contribute the majority of streamflow during baseflow periods.

Regional models and conductivity predictions

Our watershed assessment of covariates that influenced SC in the RFBC watershed showed that SC was consistently related to proportion mined and, at times, to proportion forested, road density, and elevation. These findings were largely consistent with results from other studies in this region (Lindberg et al. 2011, Bernhardt et al. 2012, Cormier et al. 2013, Merriam et al. 2015b). We found that proportion mined had a positive relationship with SC, and others who have also used NAIP aerial imagery have similarly observed such a relationship (Lindberg et al. 2011, Merriam et al. 2015b). However, we also observed a curvilinear relationship between SC and proportion mined, which was illustrated in the case of monitoring site FMB, the site with the highest levels of measured SC in 7 of the 8 monitoring periods. FMB had a proportion mined of 0.24, whereas 4 sites with greater proportion mined, up to 0.30, were found to have slightly-lower SC measurements. The FMB site has long-term active mining operations including a processing plant and coal refuse/waste pond within the catchment with outfalls in or near the stream. Coal processing areas and waste refuse storage effluents often have high SC levels that discharge from outfalls on a consistent basis. These discharge sources within the FMB catchment may help explain how lower proportion mined can have higher stream SC when compared to other catchments with more proportion mined. The 4 sites with higher proportion mined but lower SC, clustered on tributaries of Saltlick Creek in the Lower RFBC, are downstream of coal mining activities that are inactive or reclaimed. These sites also show residential development along their streams, as substantiated by NAIP imagery, and previous research has shown that catchments with combined mining and development can have lower SC than catchments with only mining (Merriam et al. 2015a). Alternatively, there could be an unmeasured covariate, such as mining-activity intensity, or an interaction affecting SC values at these sites. The quadratic form that provided good fit in our models may not produce the best fit across

other sets of sites that do not have this complex pattern of land use.

The associations of forests, roads, and elevation with SC were not as consistently selected in models as proportion mined, but their influences on stream SC are worth exploring. The negative relationship between SC and proportion of forest cover has previously been observed in this ecoregion (Cormier et al. 2013). Its consistent selection during high-discharge conditions could indicate that the interception of precipitation by forests and the ability of upper soil horizons in forested areas to enhance infiltration of precipitation lead to less runoff. Except in the case of saturation excess overland flow, a lower amount of runoff would then contact and weather valley fills (Evans et al. 2015), leading to lower stream SC. Elevation was often positively associated with SC in non-spatial models, which may indicate that once its variation was accounted for by spatial autocorrelation in the SSN analysis, that association was no longer detected (Ver Hoef et al. 2014). A negative relationship between elevation and SC was only detected in April 2014, the sample period with greatest discharge. This negative slope might indicate runoff contributing to SC at lower elevations during a period of maximum recorded discharge.

Benefits of spatial over non-spatial modeling

Our comparison of spatial and non-spatial modeling revealed several benefits to including spatial autocorrelation in models of stream chemistry throughout a stream network. First, SSN models allowed for partitioning of variance that was unexplained by covariates into spatial components that previous non-spatial studies were not able to address. For example, in the West Virginia, USA, portion of the CAP ecoregion, stream SC increased with increasing % catchment area mined, but ~50% of variation in SC was unexplained and was attributed to temporal variation in streamflow (Bernhardt et al. 2012; Table 6). Such temporal variation is illustrated in our results, but including spatial autocorrelation in our models also allowed for partitioning of spatial effects and detection of alternations in stream network relationships (i.e., flow-connected and flow-unconnected relationships) due to streamflow. This partitioning of spatial effects, beyond the variation attributable to covariates, can suggest mechanisms for patterns in stream chemistry, which is an advantage of SSN models (Isaak et al. 2014).

Next, including spatial autocorrelation in our models improved our ability to predict stream SC. Previous research in the CAP modeled and predicted SC as a function of multiple SC sources (i.e., surface mining, underground mining, and structure density; Table 6) but assumed independence between sites (Merriam et al. 2015b). Some slight spatial autocorrelation was detected in posteriori analysis, indicating that the inclusion of network relationships could be useful. Our incorporation of spatial autocorrelation was advantageous because our standard error estimates for both regression coefficients and SC predictions were not artificially small, which would occur had we assumed independence among sites (Cressie 1993, Legendre 1993, Krivoruchko 2011). Ignoring spatial autocorrelation's effect on stream chemistry (e.g., by assuming sites along a stream network are independent) produces predictions with smaller confidence intervals than when spatial autocorrelation is considered and, therefore, underestimates uncertainty (Krivoruchuko 2011). This too-narrow confidence interval is produced because its numerator only contains the standard deviation. In contrast,

Table 6. Characteristics of regional studies that examined relationships between specific conductivity and land use and land cover (LULC) in the Central Appalachian ecoregion. NAIP = National Agricultural Imagery Program, NLCD = National Land Cover Database, MLR = multiple linear regression, NPDES = National Pollutant Discharge Elimination System, SLR = simple linear regression, SSN = spatial stream network, WVSAMB = West Virginia State Address Mapping Board.

Study characteristics	Bernhardt et al. 2012	Merriam et al. 2015b	This study
Duration of stream site measurements	1997–2007, Spring–Summer (April–August)	2010–2011, Summer (July–August)	2012–2014, quarterly sampling
LULC data source and time span	Landsat (1976, 1985, 1995, 2005), NLCD (2001)	NAIP (2011), NPDES permits, WVSAMB (2003)	See Table 1
SC model	SLR	MLR	SSN
Sample unit and spatial characterization	Point and contributing catchment area (<50 km^2)	Point and contributing catchment area (<40 km^2)	Point on continuous stream network (≤400 km^2)
Spatial assumption	Independent observations	Independent observations	Autocorrelated observations
Spatial extent (km^2)	19,581	20,795	400
Sample size (density)	223 (0.011 sites/km^2)	170 (0.008 sites/km^2)	60 (0.15 sites/km^2)
Stream kilometers	13,128	24,180	545
Headwaters to outlet configuration	No	No	Yes

if positive spatial autocorrelation is present, the numerator contains the product of the standard deviation and spatial autocorrelation (Cressie 1993, Legendre 1993, Krivoruchko 2011). Also, standard errors, and consequently confidence limits, of predictions from non-spatial MLR models are similar in size regardless of network position, but standard errors from SSN models show the expected kriging pattern of being smaller near monitoring sites and increasing as distances from those sites increase (Ver Hoef et al. 2006, Isaak et al. 2014).

Incorporating spatial autocorrelation also improved our ability to predict stream SC by reducing the potential for incorrectly identifying effects. Using MLR models, we detected strong associations between some covariates and SC that we did not detect with SSN models. When spatial autocorrelation was included in SSN models, some of the standard errors for those covariates' coefficients were wider, and the coefficients no longer presented an effect. This contrast in modeling outcomes suggests a false detection of effect, or Type I error, for the MLR models. Such a result has also been shown in other SSN analyses (Ver Hoef et al. 2006, 2014, Isaak et al. 2014). In addition, our SSN models both fit the data better and gave better predictions than MLR models did (as evidenced by larger AIC weights and smaller RMSPE, especially at high discharge). Similar to our findings, spatial models of conductivity in Maryland, USA, streams produced better predictions of conductivity based on smaller mean square prediction error vs non-spatial MLR (Peterson et al. 2006). Our results support that kriging methods such as SSN, which make use of the spatial characteristics of data, are preferable when sample size, spatial density, and configuration of site requirements can be met (Som et al. 2014).

Finally, our spatial models had an advantage over MLR models in their ability to handle multiple spatial relationships that occurred in stream data (Peterson and Ver Hoef 2010). Our SSN models accounted for intermediate-scale variation not incorporated through the covariates by modeling Euclidean, tail-up, and tail-down autocovariances (Peterson and Ver Hoef 2010). Implementing an SSN study design requires careful consideration of site locations at the outlet, headwaters, and confluence-based clusters to capture spatial autocorrelation at a variety of spatial scales and consideration of multiple types of distances (Peterson et al. 2006, Som et al. 2014). Our models, along with the models of Bernhardt et al. (2012) and Merriam et al. (2015b), used covariates to capture large-scale variation in SC in the CAP ecoregion. Although all 3 studies were used to spatially predict estimates of impaired stream km (Table 6), the data used for predictions by Bernhardt et al. (2012) and Merriam et al. (2015b) were based on sampled monitoring sites constrained to catchment sizes of <50 or 40 km^2, respectively, covering just part of the stream network in their larger study areas. Our predictions were based on data from monitoring sites over a large continuum of catchment sizes from 1.4 to 400 km^2, and our inclusion of spatial modeling allowed us to treat the entire stream network as continuous. We were, thus, able to integrate, or average, predictions over the entire network and detect multiple levels of spatial autocorrelation in stream SC.

Secondary salinization often occurs as a result of multiple sources within a watershed (Griffith et al. 2012, Cañedo-Argüelles et al. 2013, Moore et al. 2017, Kaushal et al. 2018). In parts of the CAP ecoregion, secondary salinization often occurs in the headwaters of stream networks. Studies that incorporate an integrative watershed assessment from headwaters to watershed outlet, through the inclusion of spatial dependence, provide a clearer understanding of salinization effects throughout the network than do studies without a spatial component. Assessments that consider the multiscale spatial relationships that can occur between the landscape and stream network can provide inference about flow-connected and flow-unconnected, as well as catchment-scale, effects of land-cover and land-use covariates (Peterson and Ver Hoef 2010). Our novel geostatistical analysis showed where and when SC exceedance of the benchmark of 300 µS/cm in the stream network would likely affect aquatic life (USEPA 2011). A strength of our study was examining how hydrologic variability altered the nature and degree of spatial autocorrelation and incorporating that autocorrelation into SC predictions. Acknowledging the unique spatial characteristics of stream ecosystems can improve freshwater research and management (Peterson and Ver Hoef 2010).

ACKNOWLEDGEMENTS

Author contributions: MGM wrote most of the manuscript and performed the data analysis. EMS, RP, and JA designed the study. JA led the on-site data collection and quality assurance and quality control of the data. ED and RP collected, managed, geoprocessed, and interpreted the geospatial data. KT provided and interpreted the permitting data. ED, EMS, RP, JA, and KT wrote subsections related to their expertise and offered constructive suggestions on drafts of the manuscripts.

The authors acknowledge Kristin Broms and Anna Springsteen of Neptune and Company for statistical support and Mark S. Murphy of CSRA for geographic information system support. Also, we thank the field crews and laboratory scientists for collecting and processing the data. We thank Ken M. Fritz, Michael B. Griffith, Charles R. Lane, and Roy W. Martin for helpful feedback on our manuscript. We thank Justicia Rhodus (Pegasus Technical Services) for manuscript editing and formatting. The information in this document has been funded entirely by the United States Environmental Protection Agency (USEPA). Pegasus Technical Services provided support in the form of salary for ED but did not have any additional role in the study design, data collection and analysis, decision to publish, or preparation of the manuscript. This paper has been subjected to USEPA peer and administrative review and approved for publication. However, the views expressed are those of the authors and do not necessarily represent the views or policies of the USEPA. The authors declare that there are no conflicts of interest. Upon publication, supporting geospatial data (stream network, observed

and predicted specific conductivity, predictor variables) will be made available at the Environmental Protection Agency Science Hub repository. See the Appendices for DOIs to specific material. The mention of equipment or trade names does not connote official endorsement by the USEPA.

LITERATURE CITED

Bernhardt, E. S., B. D. Lutz, R. S. King, J. P. Fay, C. E. Carter, A. M. Helton, D. Campagna, and J. Amos. 2012. How many mountains can we mine? Assessing the regional degradation of Central Appalachian rivers by surface coal mining. Environmental Science & Technology 46:8115–8122.

Boehme, E. A., C. E. Zipper, S. H. Schoenholtz, D. J. Soucek, and A. J. Timpano. 2016. Temporal dynamics of benthic macroinvertebrate communities and their response to elevated specific conductance in Appalachian coalfield headwater streams. Ecological Indicators 64:171–180.

Brennan, S. R., C. E. Torgersen, J. P. Hollenbeck, D. P. Fernandez, C. K. Jensen, and D. E. Schindler. 2016. Dendritic network models: Improving isoscapes and quantifying influence of landscape and in-stream processes on strontium isotopes in rivers. Geophysical Research Letters 43:5043–5051.

Cañedo-Argüelles, M., B. J. Kefford, C. Piscart, N. Prat, R. B. Schäfer, and C.-J. Schulz. 2013. Salinisation of rivers: An urgent ecological issue. Environmental Pollution 173:157–167.

Clements, W. H., and C. Kotalik. 2016. Effects of major ions on natural benthic communities: An experimental assessment of the US Environmental Protection Agency aquatic life benchmark for conductivity. Freshwater Science 35:126–138.

Cormier, S. M., S. P. Wilkes, and L. Zheng. 2013. Relationship of land use and elevated ionic strength in Appalachian watersheds. Environmental Toxicology and Chemistry 32:296–303.

Costigan, K. H., K. L. Jaeger, C. W. Goss, K. M. Fritz, and P. C. Goebel. 2016. Understanding controls on flow permanence in intermittent rivers to aid ecological research: Integrating meteorology, geology and land cover. Ecohydrology 9:1141–1153.

Cressie, N. A. C. 1993. Statistics for spatial data. John Wiley & Sons, New York, New York.

Dent, C. L., and N. B. Grimm. 1999. Spatial heterogeneity of stream water nutrient concentrations over successional time. Ecology 80:2283–2298.

Dormann, C. F., J. Elith, S. Bacher, C. Buchmann, G. Carl, G. Carré, J. R. G. Marquéz, B. Gruber, B. Lafourcade, P. J. Leitão, T. Münkemüller, C. McClean, P. E. Osborne, B. Reineking, B. Schröder, A. K. Skidmore, D. Zurell, and S. Lautenbach. 2013. Collinearity: A review of methods to deal with it and a simulation study evaluating their performance. Ecography 36:27–46.

Doyle, P. 1991. Documented autumnal streamflow increase without measurable precipitation. Journal of the American Water Resources Association 27:915–922.

Evans, D. M., C. E. Zipper, E. T. Hester, and S. H. Schoenholtz. 2015. Hydrologic effects of surface coal mining in Appalachia (US). Journal of the American Water Resources Association 51:1436–1452.

Frieden, J. C., E. E. Peterson, J. A. Webb, and P. M. Negus. 2014. Improving the predictive power of spatial statistical models of stream macroinvertebrates using weighted autocovariance functions. Environmental Modelling & Software 60:320–330.

Fritz, K. M., K. A. Schofield, L. C. Alexander, M. G. McManus, H. E. Golden, C. R. Lane, W. G. Kepner, S. D. LeDuc, J. E. DeMeester, and A. I. Pollard. 2018. Physical and chemical connectivity of streams and riparian wetlands to downstream waters: A synthesis. Journal of the American Water Resources Association 54:323–345.

Furnival, G. M., and R. W. Wilson. 1974. Regressions by leaps and bounds. Technometrics 16:499–511.

Godsey, S., and J. W. Kirchner. 2014. Dynamic, discontinuous stream networks: Hydrologically driven variations in active drainage density, flowing channels and stream order. Hydrological Processes 28:5791–5803.

Green, J., M. Passmore, and H. Childers. 2000. A survey of the condition of streams in the primary region of mountaintop mining/valley fill coal mining. Mountaintop mining/valley fill programmatic environmental impact statement. United States Environmental Protection Agency, Region III, Aquatic Biology Group, Wheeling, West Virginia. (Available from: http://www.cet.edu/pdf/mtmvfbenthics.pdf)

Griffith, M. B. 2014. Natural variation and current reference for specific conductivity and major ions in wadeable streams of the conterminous USA. Freshwater Science 33:1–17.

Griffith, M. B. 2017. Toxicological perspective on the osmoregulation and ionoregulation physiology of major ions by freshwater animals: Teleost fish, Crustacea, aquatic insects, and Mollusca. Environmental Toxicology and Chemistry 36:576–600.

Griffith, M. B., S. B. Norton, L. C. Alexander, A. I. Pollard, and S. D. LeDuc. 2012. The effects of mountaintop mines and valley fills on the physicochemical quality of stream ecosystems in the central Appalachians: A review. Science of the Total Environment 417–418:1−12.

Hartman, K. J., M. D. Kaller, J. W. Howell, and J. A. Sweka. 2005. How much do valley fills influence headwater streams? Hydrobiologia 532:91−102.

Hitt, N. P., M. Floyd, M. Compton, and K. McDonald. 2016. Threshold responses of Blackside Dace (*Chrosomus cumberlandensis*) and Kentucky Arrow Darter (*Etheostoma spilotum*) to stream conductivity. Southeastern Naturalist 15:41–60.

Isaak, D. J., E. E. Peterson, J. M. Ver Hoef, S. J. Wenger, J. A. Falke, C. E. Torgersen, C. Sowder, E. A. Steel, M. J. Fortin, C. E. Jordan, A. S. Ruesch, N. Som, and P. Monestiez. 2014. Applications of spatial statistical network models to stream data. Wiley Interdisciplinary Reviews: Water 1:277–294.

Isaak, D. J., J. M. Ver Hoef, E. E. Peterson, D. L. Horan, and D. E. Nagel. 2016. Scalable population estimates using spatial-stream-network (SSN) models, fish density surveys, and national geospatial database frameworks for streams. Canadian Journal of Fisheries and Aquatic Sciences 74:147–156.

Jhwueng, D.-C., and B. O'Meara. 2015. *BMhyd*: PCM for hybridization. (Available at: https://github.com/cran/BMhyd)

Johnson, B. R., A. Haas, and K. M. Fritz. 2010. Use of spatially explicit physicochemical data to measure downstream impacts of headwater stream disturbance. Water Resources Research 46:W09526.

Kaushal, S. S., G. E. Likens, M. L. Pace, R. M. Utz, S. Haq, J. Gorman, and M. Grese. 2018. Freshwater salinization syndrome on a

continental scale. Proceedings of the National Academy of Sciences 115:E574–E583.
Krivoruchko, K. 2011. Spatial statistical data analysis for GIS users. Environmental Systems Reseach Institute Press, Redlands, California.
Larsen, S., M. C. Bruno, I. P. Vaughan, and G. Zolezzi. 2019. Testing the River Continuum Concept with geostatistical stream-network models. Ecological Complexity 39:100773.
Legendre, P. 1993. Spatial autocorrelation: Trouble or new paradigm? Ecology 74:1659–1673.
Lindberg, T. T., E. S. Bernhardt, R. Bier, A. M. Helton, R. B. Merola, A. Vengosh, and R. T. Di Giulio. 2011. Cumulative impacts of mountaintop mining on an Appalachian watershed. Proceedings of the National Academy of Sciences 108:20929−20934.
Marsha, A., E. A. Steel, A. H. Fullerton, and C. Sowder. 2018. Monitoring riverine thermal regimes on stream networks: Insights into spatial sampling designs from the Snoqualmie River, WA. Ecological Indicators 84:11–26.
McGuire, K. J., C. E. Torgersen, G. E. Likens, D. C. Buso, W. H. Lowe, and S. W. Bailey. 2014. Network analysis reveals multiscale controls on streamwater chemistry. Proceedings of the National Academy of Sciences 111:7030–7035.
McLeod, A. I., and X. Changjiang. 2018. *bestglm*: Best subset GLM and regression utilities. (Available from: https://CRAN.R-project.org/package=bestglm)
McManus, M. G., G. J. Pond, L. Reynolds, and M. B. Griffith. 2016. Multivariate condition assessment of watersheds with linked micromaps. Journal of the American Water Resources Association 52:494–507.
Merriam, E. R., and J. T. Petty. 2016. Under siege: Isolated tributaries are threatened by regionally impaired metacommunities. Science of the Total Environment 560–561:170–178.
Merriam, E. R., J. T. Petty, G. T. Merovich, J. B. Fulton, and M. P. Strager. 2011. Additive effects of mining and residential development on stream conditions in a central Appalachian watershed. Journal of the North American Benthological Society 30: 399−418.
Merriam, E. R., J. T. Petty, M. P. Strager, A. E. Maxwell, and P. F. Ziemkiewicz. 2015a. Complex contaminant mixtures in multistressor Appalachian riverscapes. Environmental Toxicology and Chemistry 34:2603–2610.
Merriam, E. R., J. T. Petty, M. P. Strager, A. E. Maxwell, and P. F. Ziemkiewicz. 2015b. Landscape-based cumulative effects models for predicting stream response to mountaintop mining in multistressor Appalachian watersheds. Freshwater Science 34:1006–1019.
Merricks, T. C., D. S. Cherry, C. E. Zipper, R. J. Currie, and T. W. Valenti. 2007. Coal-mine hollow fill and settling pond influences on headwater streams in southern West Virginia, USA. Environmental Monitoring and Assessment 129:359–378.
Moore, J., D. L. Bird, S. K. Dobbis, and G. Woodward. 2017. Nonpoint source contributions drive elevated major ion and dissolved inorganic carbon concentrations in urban watersheds. Environmental Science & Technology Letters 4:198–204.
MRLC (Multi-Resolution Land Characteristics). 2011. NLCD 2011 land cover (CONUS). United States Geological Survey, Multi-Resolution Land Characteristics Consortium, Sioux Falls, South Dakota. (Available from: https://www.mrlc.gov/data/nlcd-2011-land-cover-conus-0, Accessed September 2016)
Nippgen, F., M. R. Ross, E. S. Bernhardt, and B. L. McGlynn. 2017. Creating a more perennial problem? Mountaintop removal coal mining enhances and sustains saline baseflows of Appalachian watersheds. Environmental Science & Technology 51:8324–8334.
Omernik, J. M. 1987. Ecoregions of the conterminous United States. Annals of the Association of American Geographers 77:118–125.
Pericak, A. A., C. J. Thomas, D. A. Kroodsma, M. F. Wasson, M. R. Ross, N. E. Clinton, D. J. Campagna, Y. Franklin, E. S. Bernhardt, and J. F. Amos. 2018. Mapping the yearly extent of surface coal mining in Central Appalachia using Landsat and Google Earth Engine. PloS ONE 13:e0197758.
Peterson, E. E., A. A. Merton, D. M. Theobald, and N. S. Urquhart. 2006. Patterns of spatial autocorrelation in stream water chemistry. Environmental Monitoring and Assessment 121:571–596.
Peterson, E. E., and J. M. Ver Hoef. 2010. A mixed-model moving-average approach to geostatistical modeling in stream networks. Ecology 91:644–651.
Peterson, E. E., and J. M. Ver Hoef. 2014. STARS: An ArcGIS toolset used to calculate the spatial information needed to fit spatial statistical models to stream network data. Journal of Statistical Software 56:1–17.
Peterson, E. E., J. M. Ver Hoef, D. J. Isaak, J. A. Falke, M.-J. Fortin, C. E. Jordan, K. McNyset, P. Monestiez, A. S. Ruesch, A. Sengupta, N. Som, E. A. Steel, D. M. Theobald, C. E. Torgersen, and S. J. Wenger. 2013. Modelling dendritic ecological networks in space: An integrated network perspective. Ecology Letters 16:707–719.
Pond, G. J., M. E. Passmore, F. A. Borsuk, L. Reynolds, and C. J. Rose. 2008. Downstream effects of mountaintop coal mining: Comparing biological conditions using family- and genus-level macroinvertebrate bioassessment tools. Journal of the North American Benthological Society 27:717−737.
Pond, G. J., M. E. Passmore, N. D. Pointon, J. K. Felbinger, C. A. Walker, K. J. Krock, J. B. Fulton, and W. L. Nash. 2014. Long-term impacts on macroinvertebrates downstream of reclaimed mountaintop mining valley fills in Central Appalachia. Environmental Management 54:919–933.
Ramsey, F., and D. Schafer. 2002. The statistical sleuth: A course in methods of data analysis. 2nd edition. Duxbury Press, Belmont, California.
Rushworth, A. M., E. E. Peterson, J. M. Ver Hoef, and A. W. Bowman. 2015. Validation and comparison of geostatistical and spline models for spatial stream networks. Environmetrics 26:327–338.
Scown, M. W., M. G. McManus, J. H. Carson, and C. T. Nietch. 2017. Improving predictive models of in-stream phosphorus based on nationally-available spatial data coverages in a Southwestern Ohio watershed. Journal of the American Water Resources Association 53:944–960.
Slack, K. V., and H. R. Feltz. 1968. Tree leaf control on low flow water quality in a small Virginia stream. Environmental Science & Technology 2:126–131.
Som, N. A., P. Monestiez, J. M. Ver Hoef, D. L. Zimmerman, and E. E. Peterson. 2014. Spatial sampling on streams: Principles for inference on aquatic networks. Environmetrics 25:306–323.
Stanley, E. H., S. G. Fisher, and N. B. Grimm. 1997. Ecosystem expansion and contraction in streams. BioScience 47:427–435.

Symonds, M. R., and A. Moussalli. 2011. A brief guide to model selection, multimodel inference and model averaging in behavioural ecology using Akaike's information criterion. Behavioral Ecology and Sociobiology 65:13–21.

Timpano, A. J., S. H. Schoenholtz, D. J. Soucek, and C. E. Zipper. 2015. Salinity as a limiting factor for biological condition in mining-influenced central Appalachian headwater streams. Journal of the American Water Resources Association 51:240–250.

Timpano, A. J., S. H. Schoenholtz, D. J. Soucek, and C. E. Zipper. 2018a. Benthic macroinvertebrate community response to salinization in headwater streams in Appalachia USA over multiple years. Ecological Indicators 91:645–656.

Timpano, A. J., C. E. Zipper, D. J. Soucek, and S. H. Schoenholtz. 2018b. Seasonal pattern of anthropogenic salinization in temperate forested headwater streams. Water Research 133:8–18.

USCB (United States Census Bureau). 2010. Cartographic Boundary Files - Shapefile. United States Census Bureau, United States Department of Commerce, Washington, DC. (Available from: https://www.census.gov/geographies/mapping-files/time-series/geo/carto-boundary-file.html, Accessed August 2016)

USCB (United States Census Bureau). 2016. TIGER/Line shapefiles. United States Census Bureau, United States Department of Commerce, Washington, DC. (Available from: https://www.census.gov/geo/maps-data/data/tiger-line.html, Accessed September 2016)

USDA (United States Department of Agriculture). 2010. USDA-FSA-APFO Digital Ortho Mosaic, 1 meter. Aerial Photography Field Office, Salt Lake City, Utah. Data hosted by United States Geological Survey, Reston, Virginia. (Available from: https://earthexplorer.usgs.gov/, Accessed June 2012)

USEPA (United States Environmental Protection Agency). 2011. A field-based aquatic life benchmark for conductivity in Central Appalachian streams (Final Report). Technical Report EPA/600/R-10/023F. United States Environmental Protection Agency, Office of Research and Development, National Center for Environmental Assessment, Washington, DC. (Available from: https://cfpub.epa.gov/ncea/risk/recordisplay.cfm?deid=233809)

USEPA (United States Environmental Protection Agency). 2019. EnviroAtlas—Dasymetric population by 12-Digit HUC for the conterminous United States. United States Environmental Protection Agency, Research Triangle Park, North Carolina. (Available from: https://edg.epa.gov/metadata/catalog/search/resource/details.page?uuid=%7B2419b680-9fec-4c8c-8516-302206d3be4c%7D, Accessed May 2019)

USGS (United States Geological Survey). 2013. The National Map, National Geospatial Program, United States Department of Interior, United States Geological Survey, Washington, DC. (Available from: https://nationalmap.gov/elevation.html, Accessed August 2016)

USGS (United States Geological Survey). 2016. NHD High Resolution. United States Department of Interior, United States Geological Survey, Reston, Virginia. (Available from: https://www.usgs.gov/core-science-systems/ngp/national-hydrography/access-national-hydrography-products, Accessed July 2016)

Ver Hoef, J. M., and E. E. Peterson. 2010. A moving average approach for spatial statistical models of stream networks. Journal of the American Statistical Association 105:6–18.

Ver Hoef, J. M., E. E. Peterson, D. Clifford, and R. Shah. 2014. *SSN*: An R package for spatial statistical modeling on stream networks. Journal of Statistical Software 56:1–45.

Ver Hoef, J. M., E. E. Peterson, and D. Theobald. 2006. Spatial statistical models that use flow and stream distance. Environmental and Ecological Statistics 13:449−464.

Voss, K. A., and E. S. Bernhardt. 2017. Effects of mountaintop removal coal mining on the diversity and secondary productivity of Appalachian rivers. Limnology and Oceanography 62:1754–1770.

SUPPLEMENTAL MATERIALS

Appendix S1. A zipped folder containing files of: 1) an html file, FWSci_Html_S1.html, showing the analytical workflow for the multiple linear regression analysis; 2) the R code, FWSci_Html_S1.Rmd; 3) data, FWSci_Model_Fit_Data_20200424.RData; and 4) data dictionary providing the covariates, their data sources, and variable names used in R coding. Available at the Environmental Protection Agency Science Hub repository (https://doi.org/ 10.23719/1518672).

Appendix S2. A zipped folder containing files of: 1) an html file, FWSci_Html_S2.html, showing the analytical workflow for the spatial stream network (SSN) analysis; 2) the R code, FWSci_Html_S2.Rmd; and 3) data, FWSci_Model_Predict_Data_20200424.RData. Available at the Environmental Protection Agency Science Hub repository (https://doi.org/10.23719/1518673).

Appendix S3. Akaike information criterion and root mean square prediction error values, and other statistics, for the 15 autocovariance models evaluated in each of the 8 sampling periods, FWSci_TableS1 SSN_ModelSelectStats.csv. Available at the Environmental Protection Agency Science Hub repository (https://doi.org/10.23719/1518570).

Fig. S1. Block-kriged predictions and 95% prediction limits at the 60 monitoring sites for each of the 8 sampling periods: December 2012 to August 2013 (A) and November 2013 to August 2014 (B). The monitoring site names are on the left-hand side of the plots and are hydrologically ordered with the station furthest upstream, ISF, at the top, and the outlet of the watershed, RFBC1, at the bottom. The Upper, Middle, and Lower on the right-hand side indicate the 3 subwatersheds. Tributaries with only a single monitoring site are in gray, whereas major tributaries and the mainstem with multiple sites are in non-gray colors, with stations on the same tributary or mainstem assigned the same color. The mainstem sites have the monitoring site name of RFBC and are listed as Mainstem in the Stream Sites legend. The other names listed in the legend are major tributaries (Ck = Creek, Fk = Fork). The colored dot (no outline) is the block-kriged specific conductivity with its 95% prediction interval shown as a horizontal line. The colored dot with the black outline is the observed value at that site. The black vertical line is at 300μS/cm, which is the specific conductivity benchmark for the Central Appalachian region. Available at the Environmental Protection Agency Science Hub repository (https://doi.org/10.23719/1518674).